# Theoretical analysis of wavelength response and electrode optimization for SOA based optical inline detector

P. MANIMARAN*, M. GANESH MADHAN[a]
*Department of Electronics Engineering, Madras Institute of Technology Campus, Anna University, Chennai - 44, India*

The wavelength response of 1.55 μm Near Traveling Wave Semiconductor Optical Amplifier(NTWSOA) based optical inline detector is reported in this paper. Three schemes of detection viz, single full length electrode, short single electrode and differential electrode are compared. Optimization of the electrode length and position in the case of differential electrode has provided significant improvement in the detection voltage and responsivity than the other schemes. The short single length electrode detection scheme provides better linearity characterstics than the other two schemes, along with a nominal value of detection voltage and responsivity. The optimum differential detection scheme, is found to provide an improvement of 6.98dB and 7.05 dB for 1550 nm and 1560 nm respectively compared to single short length elctrode scheme. It also provides 22.44 dB and 21.6 dB improvement in detected voltage compared to full length electrode detection scheme respectively, at -10 dBm input power.

(Received December 6, 2013; accepted May 15, 2014)

*Keywords*: Differential detection, Modelling, Inline detection, NTW-SOA, Electrode structure, ITU-C band

## 1. Introduction

Semiconductor Optical Amplifier (SOA) has occupied a key position in mordern optical communications. It has proved its versatility in optical links, due to its multifunctional capabilities such as amplification, inline detection, modulation, wavelength conversion and optical switching [1]. SOA also finds its applications in WDM (spectrum sliced) and CDMA (course) networks and found suitable for Opto-Electronic integrated circuits (OEIC).Conventional detectors converts the optical signal to electrical by completely obsorbing the incident optical signal. However the SOA inline detectors both amplify and detect optical signal.

Eliseev etal[1] have registered about the functional capabilities of NTW-SOA. Koai and Olshansky have reported about the amplification and simultaneous detection in SOA [2]. Rampone etal [3] made an exhaustive study on the in line detection function under single, two and three electrode structure, with preservation of dc component in NTW-SOA structure. They inferred that, differential detection scheme with three electrode mechanism gave better detected voltage and responsivity than the two electrode mechanism. Fortenberry [4] have reported about the improvement of detection voltage as the electrode is split into to sections. Eszter Udvary etal [5] have made a study on SOA based inline detector for RoF applications. Various models were developed, such as the transmission line model, traveling wave model and equivalent circuit approach, [6,7,8] to analyse the different parameters governing the SOA operation. A wideband numerical model for NTW-SOA, reported by Connelly [9], incorporates spatial variations of photon density, forward and reverse traveling ASE. Mathlouthi etal have proposed the dynamic reservoir model [10] for semiconductor optical amplifier for WDM applications. Recently an efficient electrode structure for semiconductor optical amplifier based inline detector is reported in the literature [11]. From the literature reviewed, it is obsereved that a great deal of work has been done in SOA, however the wavelength response characterstics of inline detection has not been investigated throughly.

The main theme of this paper lies in throwing light on the wavelength response of the SOA used as inline detector. A Fermi level based comprehensive model [9] which incorporates the variations in material gain with respect to change in wavelength and carrier density spatially would be more appropriate for investigation of inline detection. Also optimum electrode position and length along the active region of the device could be determined for maximum detection voltage and responsivity, if the spatial variations of carrier density characteristics of the device are known. For our analysis we use the wideband model for 1.55 μm TWSOA of connelly, which takes in to account all the essential parameters like carrier density, photon densities and ASE (forward and reverse) along the length of the device. Further, the overall gain and material gain is derived from the fermi levels of the device incorporating the influence of optical wavelegnth on these parameters, which could complement the inline detection analysis. Based on this detailed model, performance analysis for ITU grid wavelength range of 1500 nm – 1600 nm for C-band, is carried out for NT-SOA inline detector.

## 2. Device modeling

The traveling wave equation considering both the forward and reverse traveling, signal fields, ASE and carrier densities in a TWSOA is as follows [9]. The spatially varying signal field component inside the amplifier can be given as two complex traveling-waves, $E_{s_k}^{+}(z)$ and, $E_{s_k}^{-}(z)$ propagating in the positive and negative directions, respectively (1)-(4).

$$\frac{dE_{s_k}^{+}(z)}{dz}=\left(-j\beta_k+\frac{1}{2}\left(\Gamma g_m\left(\nu_k,n\right)-\alpha(n)\right)\right)E_{s_k}^{+}(z) \quad (1)$$

$$\frac{dE_{s_k}^{-}(z)}{dz}=\left(j\beta_k-\frac{1}{2}\left(\Gamma g_m\left(\nu_k,n\right)-\alpha(n)\right)\right)E_{s_k}^{-}(z) \quad (2)$$

$$\frac{dN_j^{+}(z)}{dz}=\left(\Gamma g_m\left(\nu_j,n\right)-\alpha(n)\right)N_j^{+}+R_{sp}\left(\nu_j,n\right) \quad (3)$$

$$\frac{dN_j^{-}(z)}{dz}=-\left(\Gamma g_m\left(\nu_j,n\right)-\alpha(n)\right)N_j^{-}+R_{sp}\left(\nu_j,n\right) \quad (4)$$

$$\begin{aligned}\frac{dn(z)}{dt}&=\frac{I}{edLW}-R(n(z))\\&-\frac{\Gamma}{dw}\{\sum_{k=1}^{N_s}g_m(\nu_k,n(z))(N_{sk}^{+}(z)+N_{sk}^{-}(z))\}\\&-\frac{2\Gamma}{dw}\{\sum_{k=1}^{N_m-1}g_m(\nu_k,n(z))K_j((N_j^{+}(z)+N_j^{-}(z)))\}\end{aligned} \quad (5)$$

Where $R(n(z))$ - recombination rate , $N_{s_k}^{+}=\left|E_{s_k}^{+}\right|^2$ and $N_{s_k}^{-}=\left|E_{s_k}^{-}\right|^2$ the amplitude squared of modulus of the signal field travelling wave is the photon rate ($s^{-1}$) of the wave. $N_j^{+}(z)$ and $N_j^{-}(z)$ are the spontaneous emission photon rates ($s^{-1}$)

The material gain ($g_m$) calculation in this model incorporates the carrier density variation due to band gap change and Fermi Dirac distributions in the conduction and valence bands. The dependence of material gain on λ could be shown by replacing $\nu$ with λ, where $\lambda=\frac{c}{\nu}$

The material gain is expressed as,

$$\begin{aligned}g_m(\lambda,n)=&\frac{\lambda^2}{4\sqrt{2}\pi^{3/2}n_1^{\,2}\tau}\left(\frac{2m_e m_{hh}}{\hbar(m_e+m_{hh})}\right)^{\frac{3}{2}}\\&x\sqrt{\frac{c}{\lambda}-\frac{E_g(n)}{h}}\left(f_c(\lambda)-f_v(\lambda)\right)\end{aligned} \quad (6)$$

The material gain comprises of the following two terms,

$$g_m(\lambda,n)=g_m'(\lambda)-g_m''(\lambda) \quad (7)$$

Where, $g_m'$, $g_m''$ represent the gain coefficient and the absorption coefficient respectively. They are given by

$$\begin{aligned}g_m'(\lambda)=&\frac{\lambda^2}{4\sqrt{2}\pi^{3/2}n_1^{\,2}\tau}\left(\frac{2m_e m_{hh}}{\hbar(m_e+m_{hh})}\right)^{\frac{3}{2}}\\&x\sqrt{\frac{c}{\lambda}-\frac{E_g(n)}{h}}f_c(\lambda)\left(1-f_v(\lambda)\right)\end{aligned} \quad (8)$$

$$\begin{aligned}g_m''(\lambda)=&\frac{\lambda^2}{4\sqrt{2}\pi^{3/2}n_1^{\,2}\tau}\left(\frac{2m_e m_{hh}}{\hbar(m_e+m_{hh})}\right)^{\frac{3}{2}}\\&x\sqrt{\frac{c}{\lambda}-\frac{E_g(n)}{h}}\left(1-f_c(\lambda)\right)f_v(\lambda)\end{aligned} \quad (9)$$

Where, 'c' is speed of light, 'ν' is optical frequency, '$\tau$' is radiative carrier recombination lifetime, 'n' is conduction band carrier density, '$f_c(\nu)$' is fermi-Dirac distribution in the conduction band, '$f_v(\nu)$' is fermi-Dirac distribution in the valence band and '$E_g(n)$' is band gap energy.

## 3. Detection process

The equations from (6) – (9) show the wavelength dependent material gain of the device and hence the detected voltage is expected to vary with respect to wavelength of the input signal and could be given by the equation below, [9]

$$V_\phi(\lambda,z)=(E_{fc}-E_{fv})e^{-1} \quad (10)$$

$$E_{fc}=(\ln\ \delta+\delta(64+0.05524\delta(64+\sqrt{\delta}))^{-1/4})kT \quad (11)$$

$$E_{fv}=-(\ln\ \varepsilon+\varepsilon(64+0.05524\varepsilon(64+\sqrt{\varepsilon}))^{-1/4})kT \quad (12)$$

The responsivity of the inline detector is defined as [3]

$$R_p(\lambda,z)=\frac{V_\phi(\lambda,z)}{P_{in}} \quad (13)$$

Where, $k$ - Boltzman constant, $T$ - Absolute temperature, $P_{in}$ - Input optical Power in Watts and $R_p$ - Responsivity in V/W.

As the input optical signal enters the front facet it gets amplified and sent out through the opposite facet. The voltage developed due to carrier density variations along the length of SOA for various wavelengths at different power levels, for various bias currents are determined under the full length single electrode, short electrode and differential detection schemes. The device parameters are listed in Table 1.

*Table 1. NTW-SOA Parameters [9].*

| Symbol | Parameter | Value |
|---|---|---|
| $L_c$ | Central active region length | 450 µm |
| $L_t$ | Tapered active region length | 50 µm |
| d | Active region Thickness | 0.4 µm |
| W | central active region width | 0.4 µm |
| $\Gamma$ | Confinement factor | 0.45 |
| $K_g$ | Band gap shrinkage coefficient | $0.9 \times 10^{-10}$ eVm |
| $n_1$ | InGaAsP active region Refractive Index | 3.22 |
| $n_2$ | InP region Refractive index | 3.167 |
| $dn_1/dn$ | Differential of active region RI change with respect to carrier density | $-1.8 \times 10^{-26}$ $m^{-3}$ |
| $n_{eq0}$ | Equivalent RI at zero carrier density | 3.22 |
| $dn_{eq}/dn$ | Differential of equivalent RI of active region change | $-1.34 \times 10^{-26} m^{-3}$ |
| $\eta_{in}\eta_{out}$ | input and output coupling loss | 3 dB |
| $R_1$ , $R_2$ | Input, output Reflectivity | $5 \times 10^{-5}$ |
| $K_0$ | independent loss coefficient | 6200 $m^{-1}$ |
| $K_1$ | dependent loss coefficient | 7500 $m^2$ |
| $A_{rad}$ | linear radiative recombination coefficient | $1 \times 10^7$ $s^{-1}$ |
| $B_{rad}$ | bimolecular radiative recombination coefficient | $5.6 \times 10^{-16} m^3 s^{-1}$ |
| $C_{aug}$ | auger recombination coefficient | $3 \times 10^{-41}$ $m^6 s^{-1}$ |
| $D_{leak}$ | leakage recombination coefficient | $0.0 \times 10^{-48}$ $m^{13.5} s^{-1}$ |
| $A_{nrad}$ | linear non radiative recombination coefficient | $3.5 \times 10^8$ $s^{-1}$ |
| $N_T$ | carrier density at threshold | $4.5 \times 10^{22}$ $/m^3$ |

## 4. Simulation results and discussion

### 4.1 Device characteristics

In this work the equations (1) – (9) are solved using Finite difference technique and the solutions for the carrier densities are calculated spatially over the length of the active region of the device. The length of the NTW-SOA is spatially sliced into 100 equal sections.The calculations are repeated for various wavelengths of ITU grid. The plot seen in Fig. 1, shows the variation of carrier density and gain co-efficient for various wavelengths. It is observed that the value of carrier density and gain is maximum between the 1550 nm – 1560 nm, at the bias level of 100 mA, in the absence of the input optical power.These results are in accordance with results reported by Mathluothi etal [10], for SOA in amplifier mode and hence validates our simulation process.

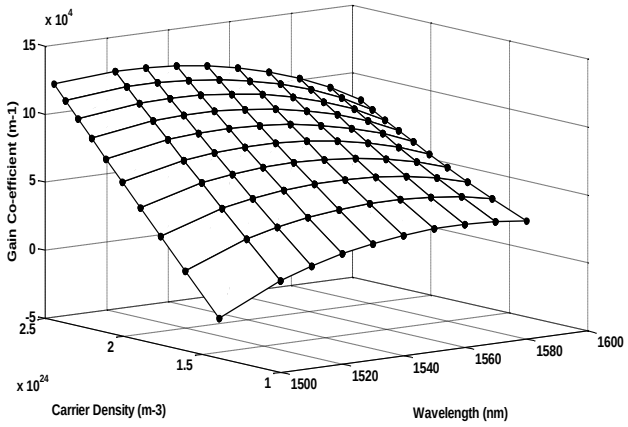


*Fig. 1. 3D-Representation of Gain co-efficient versus carrier density as a function of wavelength.*

The carrier density versus gain co-efficient characteristic is seen in Fig. 2, which shows a linear variation at all wavelengths. Fig. 3, shows the unsaturated gain for various wavelengths for different bias currents ranging from 30 mA to 120 mA at -20 dBm of input optical power. It is observed that the gain peaks around 1560 nm and lowers further for higher wavelengths and the gain also increases with bias current for all wavelengths.

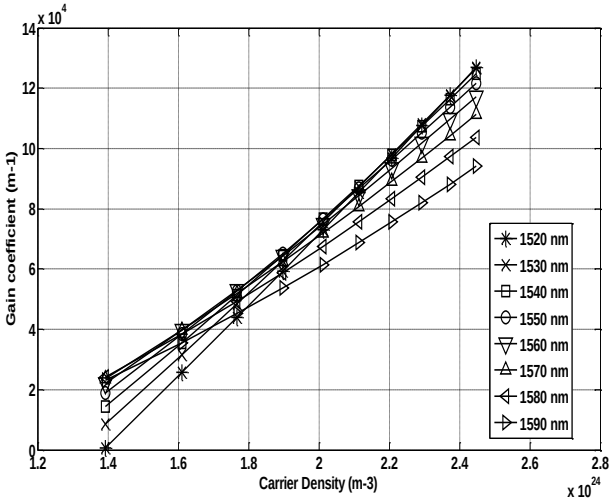


*Fig. 2. Gain co-efficient versus carrier density.*

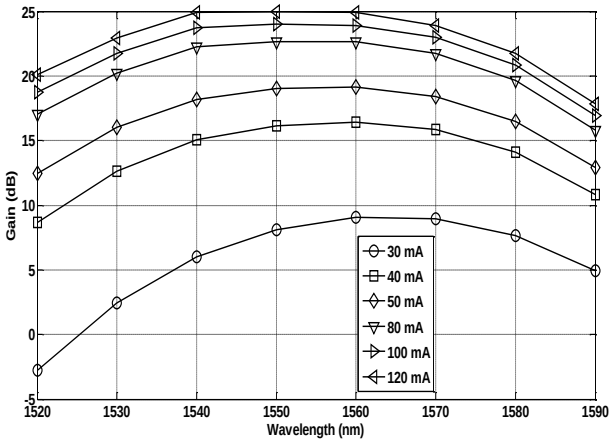


*Fig. 3. Gain versus wavelength as a function of bias currents.*

The fiber to fiber gain is plotted against wavelength as seen in Fig. 4, for a bias current of 100 mA. It is seen that the gain drops for higher values of optical power. The results observed in Fig. (2-4) are in accordance with the literature [10] and hence validates our evaluation procedure.

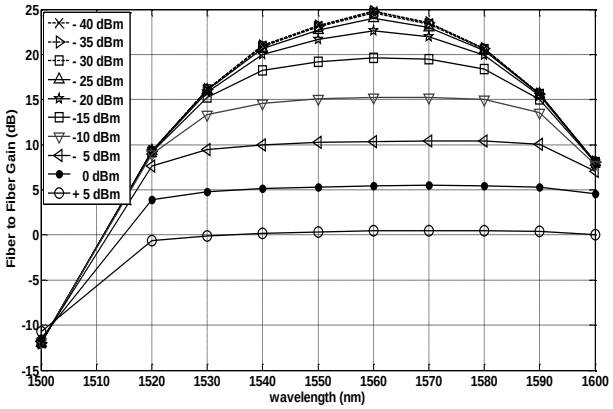


*Fig. 4. Fiber to fiber Gain versus wavelength as a function of Input optical power.*

### 4.2 Full length electrode detection scheme

In the full length electrode detection an electrode is fixed over the entire active region of the device Fig. 5, shows the detected voltages for input optical powers ranging from – 20 dBm to + 5 dBm. The bias current is fixed at 100 mA for this simulations. It is observed that the detected voltage increases with wavelength and reaches a maximum at 1570 nm and decreases beyond that. However the detected voltage is less for lower optical power for all wavelengths as seen in the Fig. 5.

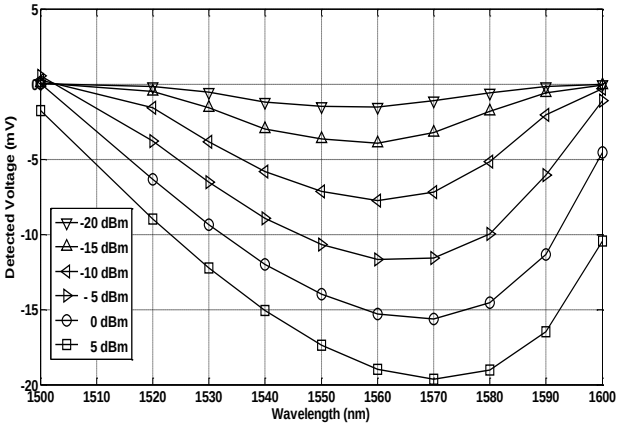


*Fig. 5. Detected voltage versus wavelength of single electrode as function of optical powers.*

The responsivity of the full length electrode structure follows the trend similar to detected voltage graph (Fig. 6). The responsivity is found to be maximum for 1560 nm and it is found to be high at lower power levels.

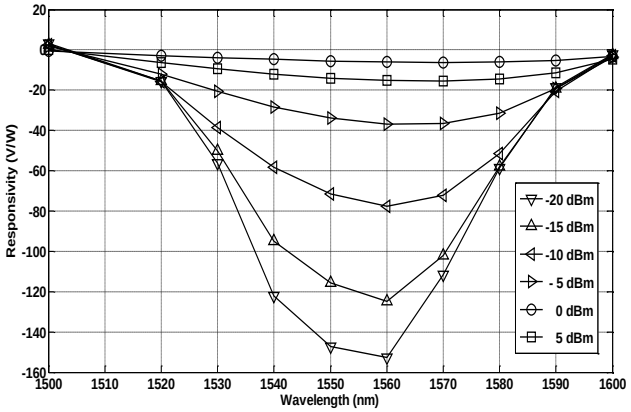


*Fig. 6. Responsivity versus wavelength of single electrode as function of optical powers.*

### 4.3 Single short length electrode detection scheme

In this detection scheme, a short length electrode is kept at a specific position in the active region corresponding to maximum variation of carrier density. The electrode structure is realised as discussed in the literature [11]. As the maximum variations in carrier density occurs in the region between 200 µm – 300 µm (Fig. 7), a single short electrode of 100 µm length is kept over this specified region, which is envisaged to provide a better detection voltage.

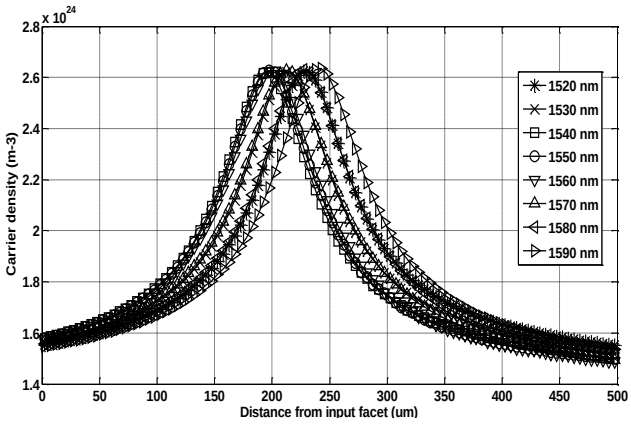


*Fig. 7. Carrier density profile along the length of device as function wavelengths for -40 dBm input power.*

Fig. 8, shows the variations of detected voltage with respect to different wavelengths for various input optical power levels. Futher it is apparent from the observations that higher power levels have higher detection voltage than lower power levels irrespective of the wavelength. It is clear that the detected voltage depends on the wavelength of the input optical signal and is found to be maximum for 1570 nm for different input power levels. For semiconductor amplifying medium, the gain is proportional to the carrier density. It is well known that the gain peak shifts towards the lower wavelengths (higher photon energy) for higher carrier density [12]. An analysis carried out in SOA, with increasing injection currents, shows the peak shift towards lower wavelength (not shown in manuscript) which also coincides with the literature. This process is reversed, as the carrier densities are depleted by higher input optical powers and the peak value of detected voltage shifts towards the longer wavelength, which is observed in Fig. 8.

The detected voltage for the short length electrode scheme for various input power levels at 1550 nm wavelength is reported in literature [11]. It is found to provide linear increase in detected voltage for increase in input power levels, which is due an uniform carrier density variation, at 200-300 µm length, for a given bias current. A similar response is obtained for different wavelengths in the case of short single electrode, which ensures linearity of this scheme. Whereas in the case of full length electrode, the variation is linear with reduced magnitude of detected voltage.

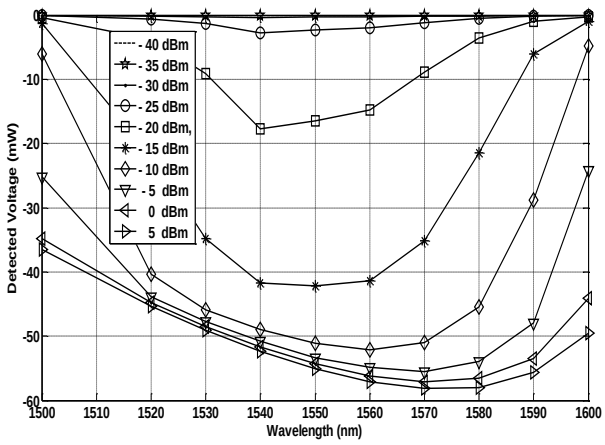


*Fig. 8. Detected voltage versus wavelength as a function of optical powers.*

The responsivity of the detector is shown in Fig. 9, where a better response is observed for wavelength between 1540-1570 nm, at lower input optical powers. Further it provides comparitively higher responsivity value for higher powers and peaks for between 1560 - 1570 nm and reduces futher a for higher wavelengths. This is due to the fact that the reponsivity of the photo detector increases with increase in wavelength as the electron density is high for the power of the input optical signal, but it does not carry on in the linear fashion as the photon energy becomes too small to generate electrons futher [12].

In comparision with the full length electrode, this scheme seems to be better in terms of both detection voltage as well as responsivity .For example in the case of 1540 nm at -15 dBm, the responsivity is around -1300 V/W, whereas in the full length single electrode case it is predicted as -95 V/W only. For the same conditions the detected voltage under short single electrode, full length electrodes is obtained as -42 mV, -

3 mV respectiviely.

Fig. 10, is the three dimentional mesh representation of Fig. 8, showing the dependance of detected voltage on wavelength and optical input power.

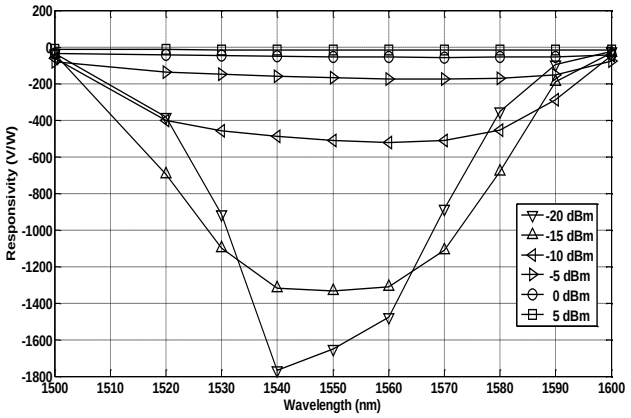


*Fig. 9. Responsivity versus wavelength as a function of optical powers.*

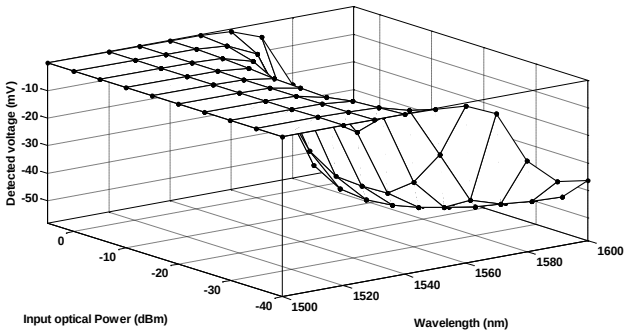


*Fig. 10. 3D-Representation of detected voltage variation as a function of wavelengths.*

### 4.4 Optimum differential detection scheme

The differential detection is not a new technique for detection of optical signals. This concept was already reported by Rampone etal, [3] where they consider two electrodes structure namely reference (Lr) and signal electrode (Ls) and the detected voltage is the difference between the voltages developed between the two electrodes and is given by the following equation,

$$V_{d\phi}(z) = V_{s\phi}(z) - V_{l\phi}(z) \tag{10}$$

But the main idea of this paper lies in the arrangement of the two electrodes such that a maximum voltage being detected out proportionally for all input optical powers. In our earlier report we have optimized the location of electrodes for maximum detected voltage by considering the carrier density profile [11]. In this proposed scheme, the detected voltage profile (Fig. 11) is taken into consideration rather than the carrier density profile. Two electrode lengths are being fixed such that one electrode lies over the positive region ( $L_p$ ) of the profile and other over the negative region ( $L_n$ ).The detected voltage is given by the following equation,

$$V_{d\phi}(z,\lambda) = V_{n\phi}(z,\lambda) - V_{p\phi}(z,\lambda) \tag{11}$$

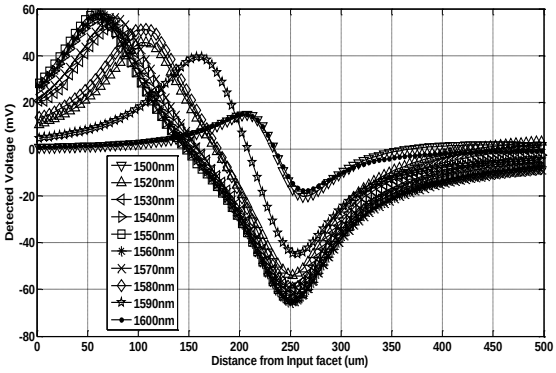


*Fig. 11. Detected voltage profile along the entire length of the device for various wavelengths.*

An algorithm is developed to identify the optimum position and length of the two electrodes so as to extract the maximum detected voltage using differential scheme. The flow chart of the algorithm is shown in the Fig. 12, the input to the algorithm are wavelength (λ), length (L), bias current (I), input power ($P_{in}$) , detected voltage ($V_{de}$) for the entire length of the active region, lengths of $L_p$ and $L_n$ and the initial positions of the respective electrodes ( $P_p = 5\mu m$ and $P_n = 500\mu m$ ). The differential detected voltage $V_{d\phi}$ is calculated using the equation 11. The positions of the respective electrodes $P_p$ is incremented and $P_n$ is decremented for which $V_{d\phi}$ computed till $P_p$ and $P_n = 250\mu m$ that is till the mid point of the active region. Finally the length and positions are fixed for which differential detected voltage $V_{d\phi}$ is maximum. The above sequence is repeated for different lengths of both the electrodes (50 µm, 75 µm, 100 µm, 150 µm) and it as found that the optimum length for both the electrodes is 50µm and position of $L_p$ is 1- 50 µm and $L_n$ is 250 µm to 300 µm. This arrangement is shown in Fig. 13.

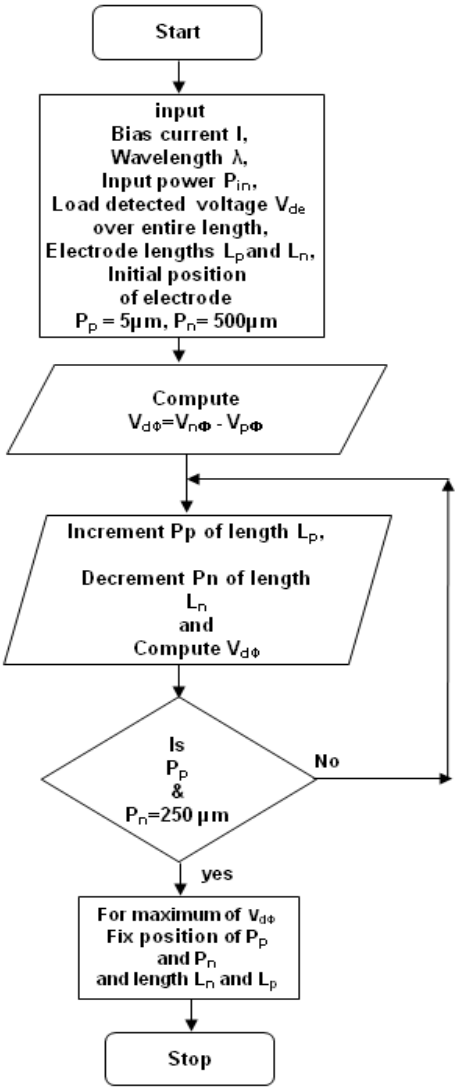


*Fig. 12. Algorithm to fix length and position of electrodes.*

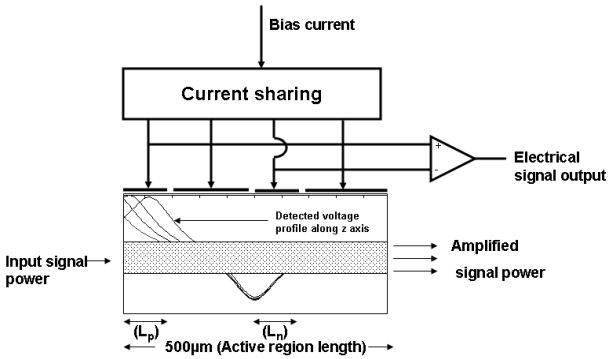


*Fig. 13. Proposed Optimum Differential detection scheme.*

It is clear from the Fig. 14, that the detected voltage shows a large improvement than the previous scheme (Fig. 8). For example, for the input power of -10 dBm at 1550 nm, the detected voltage measures about -94.12 mV whereas for single short electrode scheme it is only -42.1 mV. For higher powers ranging from 0 dBm to 5 dBm, detected voltage is found to decrease. This phenomenon is due to carrier depletion at higher input powers and shift of voltage profile (Fig. 11) towards the input facet of the device. All the wavelengths considered for the study under goes similar effect. Hence a reduction in detected voltage is observed for higher input powers at all wavelengths. However it could be noted that the detected voltage for higher powers are significantly greater compared to the short length electrode scheme. It is also seen from Fig. 15, that responsivity has also improved cosiderably, which provides maximum value of -3422 V/W for 1540 nm at -20 dBm input power.

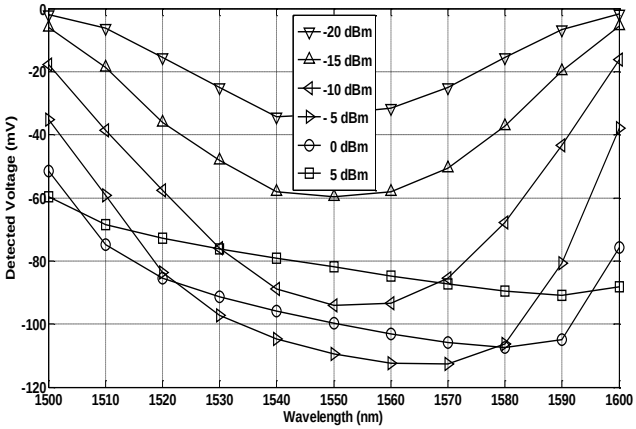


*Fig. 14. Detected voltage versus wavelength as a function of optical powers.*

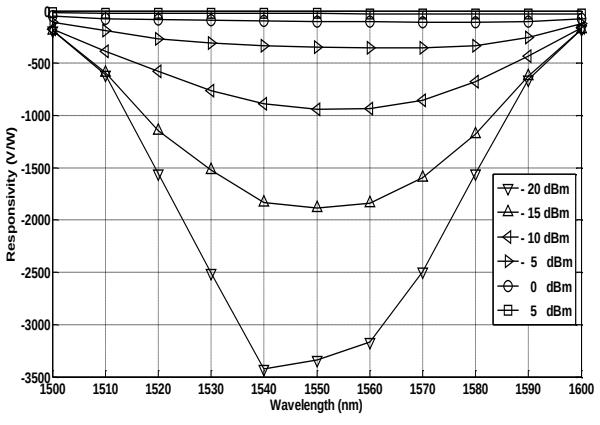


*Fig. 15. Responsivity versus wavelength as a function of optical powers.*

Table 2 gives a distinct picture of the responsivity and detected voltage of the different schemes for various wavelengths at 100 mA of bias currrent and -10 dBm input optical power. It is evident that short length electrode and optimum differential scheme are more credible than full length electrode detection. The short electrode scheme provides nominal value of detected voltage and responsivity but the linearity of this scheme

is very impressive. In the case of optimum differential detection technique the detected voltage is two fold greater than the previous scheme with comparitively higher responsivity, but less linear. Further it is also compared with the conventional two electrode differential detection scheme proposed by rampone and it is found to provide a relatively very high detected voltage and responsivity. Hence an application demanding higher linearity with average detected voltage and responsivity, can employ short length electrode scheme. But if an application requires higher detection voltage with good responsivity, then optimum differential detection scheme will be the best option.

*Table 2. Comparison of detection performance of different schemes.*

| No. | Wavelength (nm) | Full length electrode detection | | Short length electrode detection (200-300 μm) | | Optimum differential detection | | Rampone et al Differential Detection [3] | |
|---|---|---|---|---|---|---|---|---|---|
| | | Detected Voltage (mV) | Responsivity (V/W) | Detected Voltage (mV) | Responsivity (V/W) | Detected Voltage (mV) | Responsivity (V/W) | Detected Voltage (mV) | Responsivity (V/W) |
| 1. | 1500 | 0.26 | 2.6 | 6.0 | 60.5 | 17.72 | 177 | 0.05 | 0.57 |
| 2. | 1520 | 1.6 | 15.9 | 21.9 | 403.6 | 57.61 | 576 | 0.76 | 7.69 |
| 3. | 1530 | 3.9 | 38.6 | 34.8 | 459.3 | 76.15 | 759 | 1.70 | 17.06 |
| 4. | 1540 | 5.8 | 58.2 | 41.6 | 490.1 | 88.91 | 889 | 2.45 | 24.59 |
| 5 | 1550 | 7.1 | 71.6 | 42.1 | 511.4 | 94.12 | 941 | 3.36 | 33.60 |
| 6. | 1560 | 7.7 | 77.7 | 41.4 | 521.2 | 93.31 | 933 | 4.39 | 43.92 |
| 7. | 1570 | 7.2 | 72.1 | 35.2 | 510.1 | 85.42 | 854 | 5.55 | 55.50 |
| 8. | 1580 | 5.2 | 51.5 | 21.5 | 454.3 | 67.7 | 677 | 6.35 | 63.50 |
| 9. | 1590 | 2.0 | 19.3 | 6.1 | 287.8 | 43.46 | 434 | 5.11 | 51.10 |
| 10. | 1600 | 0.3 | 2.9 | 0.9 | 48.5 | 16.17 | 161 | 1.36 | 13.66 |

Tabulated for 100 mA of bias current and input optical power of -10 dBm

## 5. Conclusion

A detailed analysis of NTW-SOA based three different inline detection schemes for ITU grid wavelengths have been carried out in this paper. It is found that single short length electrode detection and optimum differential detection schemes provides significant improvement in terms of detected voltage and responsivity characteristics than the conventional full length electode scheme. The optimum differential scheme provides two fold improvement in detection voltage than the best scheme reported earlier. The short length electrode detection scheme provides higher linearity charaterstic than the other two schemes with nominal value of detection voltage and responsivity.

## References

[1] Peter G. Eliseev, Vu Van Luc, Pure Appl. Opt. 295 (1995).
[2] K. T. Koai, R. Olshansky, IEEE Photonics Tech. Lett., **4**, 441(1992).
[3] Thierry Rampone, Hong-Wu Li, Ammar Sharaiha, IEEE J. Light Wave technology, **16**, 1295 (1998).
[4] R. M. Fortenberry, A. J. Lowery, R. S.Tucker, Electronics Letters, **28**, 474 (1992).
[5] Eszter Udvary, Tibor Berceli, IEEE J. Light Wave technology, **26**, 2563 (2008).
[6] H. Ghaffouri Shiraz, Imperial college press, London, (2004).
[7] A. J. Lowery, IEE Proc. **36**, 320 (1989).
[8] M. Ganesh Madhan, R. Neelakandan, Opt Quant Electron, **40**, 535 (2008).
[9] M. J. Connelly, IEEE Journal of Quantum Electronics, **37**, 439 (2001).
[10] W. Mathlouthi, P. Lemieux, Salsi, Massimiliano, A. Vannucci, A. Bononi, L. A. Rusch, IEEE J. Light Wave technology, **24**, 4353 (2006).
[11] P. Manimaran, M. Ganesh Madhan, Optik – International Journal for Light and Electron Optics, **124**, 3842 (2013).
[12] Govind P. Agarwal, John Wiley & Sons, Inc. (2002).

*Corresponding author: maran_pm@yahoo.co.in